

Intelligent Reflecting Surface-Aided Wideband THz Communications: Modeling and Analysis

Konstantinos Dovelos[†], Stylianos D. Assimonis[†], Hien Quoc Ngo[†], Boris Bellalta^{*}, and Michail Matthaiou[†]

^{*}Department of Information and Communication Technologies, Universitat Pompeu Fabra (UPF), Barcelona, Spain

[†]Centre for Wireless Innovation (CWI), Queen’s University Belfast, Belfast, U.K.

Email: {k.dovelos, s.assimonis, hien.ngo, m.matthaiou}@qub.ac.uk, boris.bellalta@upf.edu

Abstract—In this paper, we study the performance of wideband terahertz (THz) communications assisted by an intelligent reflecting surface (IRS). Specifically, we first introduce a generalized channel model that is suitable for electrically large THz IRSs operating in the near-field. Unlike prior works, our channel model takes into account the spherical wavefront of the emitted electromagnetic waves and the spatial-wideband effect. We next show that conventional frequency-flat beamfocusing significantly reduces the power gain due to beam squint, and hence is highly suboptimal. More importantly, we analytically characterize this reduction when the spacing between adjacent reflecting elements is negligible, i.e., holographic reflecting surfaces. Numerical results corroborate our analysis and provide important insights into the design of future IRS-aided THz systems.

Index Terms—Beamfocusing, beam squint, intelligent reflecting surfaces, near-field, wideband THz communications.

I. INTRODUCTION

Unutilized spectrum resources are scarce in the sub-6 GHz band, which might limit the performance of future wireless communication systems. To this end, communication over the terahertz (THz) band (0.1 to 10 THz) is widely deemed a promising solution for beyond 5G networks due to the abundant spectrum available at those frequencies [1]. Despite the potential for terabit-per-second wireless links, THz signals can suffer from severe propagation losses because of their short wavelength. Hence, transceivers with multiple antennas, i.e., multiple-input multiple-output (MIMO), are required to mitigate those propagation losses through sharp beamforming [2]. On the other hand, the power consumption of THz radio-frequency circuits is much higher than their sub-6 GHz counterparts, which can undermine the deployment of massive antenna arrays in an energy efficient manner [3]. To surmount this challenge, the novel paradigm of IRSs can be exploited to reduce the power consumption of a single-user MIMO system, whilst fulfilling a transmission rate constraint [4]. Consequently, the performance analysis of IRS-aided THz communications is of great research importance.

As shown in [4], THz intelligent reflecting surfaces (IRSs) will likely operate in the radiating near-field where the wavefront of the emitted waves is spherical. In addition, the ultra-wide bandwidths, e.g., tens of gigahertz, of prospective THz systems along with the large number of IRS elements can yield a *spatially wideband* channel [5]. Under these circumstances, frequency-flat beamfocusing will decrease the power gain due to beam squint. To this end, [6], [7] have recently studied

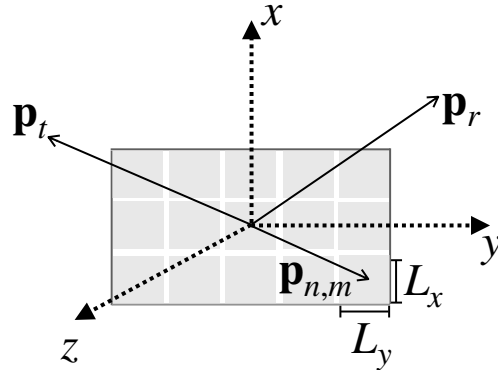


Fig. 1: Illustration of the IRS geometry under consideration.

the reflection design and channel estimation problem for IRS-aided communications in the presence of beam squint, yet considering the far-field region. To the best of our knowledge, all prior studies on IRSs (e.g., [8]–[17]) neglect the spatial-wideband effect and/or the spherical wavefront of the radiated waves. This paper aims to fill this gap in the literature, and shed light on the channel modeling and performance of IRS-assisted wideband THz communications. We commence by introducing a spherical wave channel model for discrete IRSs, which takes into account the spatial-wideband effect; note that our model includes the far-field regime as a special case. We next study the power gain under standard narrowband beamfocusing, and show that it is highly suboptimal. More importantly, we analytically evaluate the reduction in the power gain when the inter-element spacing is negligible, which corresponds to the ultimate limit of a discrete IRS known as *holographic reflecting surface* [17], [18]. Our performance analysis reveals that beam squint mitigation through a frequency-selective surface design is essential for reaping the full potential of IRS-assisted wideband THz systems.

Notation: Throughout the paper, \mathbf{X} is a matrix; \mathbf{x} is a vector; x and X are scalars; $(\cdot)^*$, $(\cdot)^T$, and $(\cdot)^H$ are the conjugate, transpose and conjugate transpose, respectively; $[\mathbf{X}]_{i,j}$ is the (i, j) th entry of \mathbf{X} ; $\text{vec}(\mathbf{X})$ is the column vector formed by stacking the columns of \mathbf{X} ; $\mathcal{F}\{\cdot\}$ is the continuous-time Fourier transform; $\mathbf{x} \sim \mathcal{CN}(\boldsymbol{\mu}, \boldsymbol{\Sigma})$ is a complex Gaussian vector with mean $\boldsymbol{\mu}$ and covariance matrix $\boldsymbol{\Sigma}$; and $\text{erf}(x) = \frac{2}{\sqrt{\pi}} \int_0^x e^{-t^2} dt$ is the error function.

II. CHANNEL MODEL WITH SPATIAL-WIDEBAND EFFECTS

A. System Setup

We consider an IRS-assisted THz system, where the transmitter (Tx) and receiver (Rx) have a single antenna each. The IRS is placed in the xy -plane, and it consists of $N = N_x \times N_y$ passive reflecting elements of size $L_x \times L_y$ each, as depicted in Fig. 1; the inter-element spacing is negligible and is ignored [13]. The origin of the coordinate system is placed at the center of the IRS. The position of each IRS element is measured from its center. Then, the position vector of the (n, m) th IRS element is $\mathbf{p}_{n,m} = ((n - 1/2)L_x, (m - 1/2)L_y, 0)$, for $n = -\frac{N_x}{2}, \dots, \frac{N_x}{2} - 1$, and $m = -\frac{N_y}{2}, \dots, \frac{N_y}{2} - 1$. Likewise, $\mathbf{p}_t = (r_t, \theta_t, \phi_t)$ and $\mathbf{p}_r = (r_r, \theta_r, \phi_r)$ are the position vectors of the Tx and Rx, respectively, where r is the radial distance, θ is the polar angle, and ϕ is the azimuth angle. In Cartesian coordinates, the distance between the Tx and the (n, m) th IRS element is hence given by

$$\begin{aligned} r_t(n, m) &\triangleq \|\mathbf{p}_t - \mathbf{p}_{n,m}\| \\ &= r_t \left(1 + \frac{((n - \frac{1}{2})L_x)^2}{r_t^2} - \frac{2 \cos \phi_t \sin \theta_t (n - \frac{1}{2})L_x}{r_t} \right. \\ &\quad \left. + \frac{((m - \frac{1}{2})L_y)^2}{r_t^2} - \frac{2 \sin \phi_t \sin \theta_t (m - \frac{1}{2})L_y}{r_t} \right)^{1/2}. \end{aligned} \quad (1)$$

Similarly, the distance between the Rx and the (n, m) th IRS element is calculated as

$$\begin{aligned} r_r(n, m) &\triangleq \|\mathbf{p}_r - \mathbf{p}_{n,m}\| \\ &= r_r \left(1 + \frac{((n - \frac{1}{2})L_x)^2}{r_r^2} - \frac{2 \cos \phi_r \sin \theta_r (n - \frac{1}{2})L_x}{r_r} \right. \\ &\quad \left. + \frac{((m - \frac{1}{2})L_y)^2}{r_r^2} - \frac{2 \sin \phi_r \sin \theta_r (m - \frac{1}{2})L_y}{r_r} \right)^{1/2}. \end{aligned} \quad (2)$$

B. Channel Model

We focus on the Tx-IRS-Rx link. The received baseband signal propagated through the IRS is expressed as

$$r(t) = \sum_{n=-\frac{N_x}{2}}^{\frac{N_x}{2}-1} \sum_{m=-\frac{N_y}{2}}^{\frac{N_y}{2}-1} h_{n,m} e^{j\varphi_{n,m}} x(t - \tau_{n,m}) + \tilde{n}(t), \quad (3)$$

where $e^{j\varphi_{n,m}}$, $\varphi_{n,m} \in [-\pi, \pi]$, is the reflection coefficient of the (n, m) th IRS element, $\tilde{n}(t) \sim \mathcal{CN}(0, \sigma^2)$ is the additive noise at the receive end, $x(t)$ is the transmitted baseband signal, and $\tau_{n,m}$ is the associated propagation delay given by

$$\tau_{n,m} = \frac{r_r(n, m) + r_t(n, m)}{c}, \quad (4)$$

where c denotes the speed of light. Moreover,

$$h_{n,m} = \sqrt{\text{PL}_{n,m}(f)} e^{-j2\pi f_c \tau_{n,m}} \quad (5)$$

is the cascaded channel through the (n, m) th IRS element, $\text{PL}_{n,m}(f)$ is the corresponding frequency-dependent path loss,

and f_c is the carrier frequency. The path loss of the cascaded channel through the (n, m) th IRS element is calculated as [4]

$$\begin{aligned} \text{PL}_{n,m}(f) &= \\ G_t G_r &\left(\frac{L_x L_y}{4\pi} \right)^2 \frac{F(\theta_t, \phi_r, \theta_r)}{r_t^2(n, m) r_r^2(n, m)} e^{-\kappa_{\text{abs}}(f)(r_t(n, m) + r_r(n, m))}, \end{aligned} \quad (6)$$

where $F(\theta_t, \phi_r, \theta_r) \triangleq \cos^2 \theta_t (\cos^2 \theta_r \cos^2 \phi_r + \sin^2 \phi_r)$, G_t and G_r are the Tx and Rx antenna gains, respectively, while $\kappa_{\text{abs}}(f)$ denotes the molecular absorption coefficient at frequency f [19]. Taking the Fourier transform of (3) gives

$$\begin{aligned} R(f) &\approx \sqrt{\text{PL}(f)} \underbrace{\sum_{n=-\frac{N_x}{2}}^{\frac{N_x}{2}-1} \sum_{m=-\frac{N_y}{2}}^{\frac{N_y}{2}-1} e^{-j2\pi(f_c+f)\tau_{n,m}} e^{j\varphi_{n,m}} X(f)}_{H_{\text{eff}}(f)} \\ &\quad + \tilde{N}(f), \end{aligned} \quad (7)$$

where the approximation follows from $\text{PL}_{n,m}(f) \approx \text{PL}(f)$ owing to the small physical size of THz IRSs [4], $\text{PL}(f)$ denotes the path loss calculated using the radial distances r_t and r_r , $\mathcal{F}\{r(t)\} = R(f)$, $\mathcal{F}\{x(t)\} = X(f)$, $\mathcal{F}\{\tilde{n}(t)\} = \tilde{N}(f)$, and $H_{\text{eff}}(f)$ is the effective channel accounting for the phase shifts. Note that $H_{\text{eff}}(f)$ is frequency-dependent because of the spatial-wideband effect. Next, consider orthogonal frequency division multiplexing (OFDM) modulation with S subcarriers for a signal bandwidth B . The subcarrier spacing is given by B/S , and the baseband frequency of the s th subcarrier is specified as $f_s = (s - \frac{S-1}{2}) \frac{B}{S}$, for $s = 0, \dots, S-1$. Thus, the received signal at the s th OFDM subcarrier is given by

$$R(f_s) = \sqrt{\text{PL}(f_s)} H_{\text{eff}}(f_s) X(f_s) + \tilde{N}(f_s), \quad (8)$$

where $X(f_s) \sim \mathcal{CN}(0, P_t/S)$ is the transmitted data symbol with average power P_t/S , and $\tilde{N}(f_s) \sim \mathcal{CN}(0, \sigma^2 B/S)$ is the additive noise at each subcarrier.

Remark 1 (Fresnel Approximation). *In the radiating near-field, i.e., Fresnel zone, the Tx distance can be approximated by $r_t(n, m) \approx r_t + \tilde{r}_t(n, m)$, where*

$$\begin{aligned} \tilde{r}_t(n, m) &= \frac{((n - \frac{1}{2})L_x)^2 (1 - \cos^2 \phi_t \sin^2 \theta_t)}{2r_t} \\ &\quad - \left(n - \frac{1}{2} \right) L_x \cos \phi_t \sin \theta_t \\ &\quad + \frac{((m - \frac{1}{2})L_y)^2 (1 - \sin^2 \phi_t \sin^2 \theta_t)}{2r_t} \\ &\quad - \left(m - \frac{1}{2} \right) L_y \sin \phi_t \sin \theta_t \end{aligned} \quad (9)$$

follows from the second-order Taylor polynomial $(1+x)^\alpha \approx 1 + \alpha x + \frac{1}{2} \alpha(\alpha-1)x^2$ of (1). Similarly, it holds that $r_r(n, m) \approx r_r + \tilde{r}_r(n, m)$, where $\tilde{r}_r(n, m)$ is given by (9), but θ_t , ϕ_t , and r_t are replaced by θ_r , ϕ_r , and r_r , respectively.

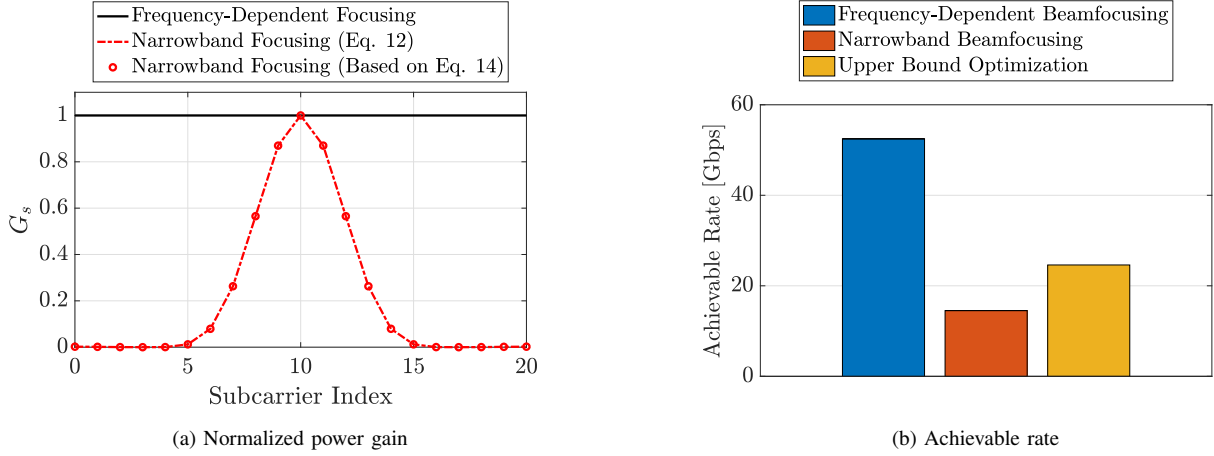


Fig. 2: Results for an 80×80 -element IRS, $B = 20$ GHz, $f_c = 300$ GHz, $(r_t, \theta_t, \phi_t) = (1, \pi/3, \pi/5)$, and $(r_r, \theta_r, \phi_r) = (5, \pi/4, \pi/3)$.

III. PERFORMANCE ANALYSIS OF IRS-AIDED WIDEBAND THZ COMMUNICATIONS

A. Power Gain

From (7), the signal-to-noise ratio (SNR) at the s th OFDM subcarrier is written as

$$\text{SNR}_s = \frac{N^2 G_s P_t \text{PL}(f_s)}{B \sigma^2}, \quad (10)$$

where $G_s \in [0, 1]$ is the normalized power gain defined as

$$G_s \triangleq \frac{|H_{\text{eff}}(f_s)|^2}{N^2}. \quad (11)$$

With frequency-dependent beamfocusing, the phase induced by the (n, m) th IRS element is $\varphi_{n,m}(f_s) = 2\pi(f_c + f_s)\tau_{n,m}$, which yields $G_s = 1$ for each OFDM subcarrier. Therefore, SNR_s grows quadratically with the number N of IRS elements. Conversely, with conventional narrowband beamfocusing, we have $\varphi_{n,m} = 2\pi f_c \tau_{n,m}$ for all subcarriers, and

$$G_s = \frac{1}{N_x^2 N_y^2} \left| \sum_{n=-\frac{N_x}{2}}^{\frac{N_x}{2}-1} \sum_{m=-\frac{N_y}{2}}^{\frac{N_y}{2}-1} e^{-j2\pi f_s \tau_{n,m}} \right|^2, \quad (12)$$

which results in $G_s < 1$ for $f_s > 0$ due to beam squint.

We next generalize the normalized power gain to the case of a holographic IRS modeled as a continuous aperture. To do so, we leverage the Fresnel approximations of $r_t(n, m)$ and $r_r(n, m)$ introduced in Remark 1. Then, (12) is recast as

$$G_s \approx \frac{1}{N_x^2 N_y^2} \left| \sum_{n=-\frac{N_x}{2}}^{\frac{N_x}{2}-1} \sum_{m=-\frac{N_y}{2}}^{\frac{N_y}{2}-1} e^{-j2\pi f_s \frac{\bar{r}_t(n,m) + \bar{r}_r(n,m)}{c}} \right|^2. \quad (13)$$

In the following proposition, we provide an analytical expression for (13).

Proposition 1 (Holographic Reflecting Surface). *The normalized power gain at the s th OFDM subcarrier is analytically evaluated as $G_s = |\xi_s|^2$, where ξ_s is given by (14) at the top*

of the next page for $k_s = 2\pi f_s/c$, $\tilde{L}_x = N_x L_x$, $\tilde{L}_y = N_y L_y$, and

$$a_x = \frac{(1 - \cos^2 \phi_t \sin^2 \theta_t)}{2r_t} + \frac{(1 - \cos^2 \phi_r \sin^2 \theta_r)}{2r_r}, \quad (15)$$

$$b_x = \cos \phi_t \sin \theta_t + \cos \phi_r \sin \theta_r, \quad (16)$$

$$a_y = \frac{(1 - \sin^2 \phi_t \sin^2 \theta_t)}{2r_t} + \frac{(1 - \sin^2 \phi_r \sin^2 \theta_r)}{2r_r}, \quad (17)$$

$$b_y = \sin \phi_t \sin \theta_t + \sin \phi_r \sin \theta_r. \quad (18)$$

Proof. See Appendix. \square

From Fig. 2(a), we observe the detrimental effect of beam squint on the normalized power gain. Moreover, we verify the excellent match between (12) and the expression in Proposition 1, which implies that a spatially continuous IRS can be accurately approximated by an ultra-dense discrete IRS.

B. Achievable Rate via Beamfocusing Optimization

To improve the system performance, we can resort to a more advanced IRS design than narrowband beamfocusing. To this end, we introduce the auxiliary matrices $\mathbf{A}_s \in \mathbb{C}^{N_x \times N_y}$, with $[\mathbf{A}_s]_{n,m} = e^{-j2\pi f_s \tau_{n,m}}$, and $\mathbf{B} \in \mathbb{C}^{N_x \times N_y}$, with $[\mathbf{B}]_{n,m} = e^{j\varphi_{n,m}}$. Then, we have $|H_{\text{eff}}(f_s)|^2 = |\mathbf{h}_s^T \mathbf{b}|^2$, where $\mathbf{h}_s = \text{vec}(\mathbf{A}_s) \in \mathbb{C}^{N \times 1}$ and $\mathbf{b} = \text{vec}(\mathbf{B}) \in \mathbb{C}^{N \times 1}$. We seek to find the reflection coefficient vector \mathbf{b} that maximizes the achievable rate, i.e.,

$$\max_{\mathbf{b}} R(\mathbf{b}) = \sum_{s=0}^{S-1} \frac{B}{S} \log_2 \left(1 + \frac{P_t \text{PL}(f_s) |\mathbf{h}_s^T \mathbf{b}|^2}{B \sigma^2} \right) \quad (19)$$

$$\text{s.t.} \quad |[\mathbf{b}]_n| = 1, \forall n = 1, \dots, N.$$

The beamfocusing optimization problem (19) resembles the wideband design problem in IRS-aided OFDM systems, which is non-convex and difficult to solve [16]. In the spirit of [16], we turn to maximize the upper bound¹ of $R(\mathbf{b})$:

$$R(\mathbf{b}) \leq B \log_2 \left(1 + \frac{P_t \text{PL}(f_s) \sum_{s=0}^{S-1} |\mathbf{h}_s^T \mathbf{b}|^2}{B \sigma^2 S} \right). \quad (20)$$

¹This optimization approach is well-established in the related literature; see [7], [16], [20], and references therein.

$$\xi_s = \frac{\pi}{4jk_s \tilde{L}_x \tilde{L}_y \sqrt{a_x a_y}} \left[\operatorname{erf} \left(\sqrt{jk_s a_x} \left(\frac{\tilde{L}_x}{2} - \frac{b_x}{2a_x} \right) \right) - \operatorname{erf} \left(\sqrt{jk_s a_x} \left(-\frac{\tilde{L}_x}{2} - \frac{b_x}{2a_x} \right) \right) \right] \times \left[\operatorname{erf} \left(\sqrt{jk_s a_y} \left(\frac{\tilde{L}_y}{2} - \frac{b_y}{2a_y} \right) \right) - \operatorname{erf} \left(\sqrt{jk_s a_y} \left(-\frac{\tilde{L}_y}{2} - \frac{b_y}{2a_y} \right) \right) \right]. \quad (14)$$

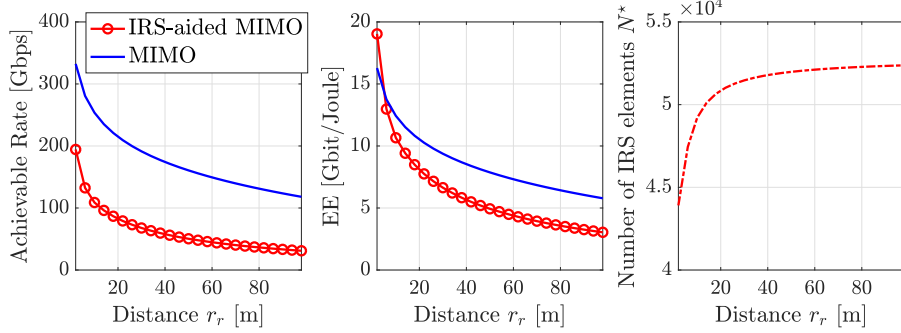


Fig. 3: Results for $\alpha = 2$, narrowband beamfocusing, and fixed IRS location at $(0,0,0)$. In the MIMO system, $N_t = 100$ and $N_r = 100$. The other parameters are $G_t = G_r = 20$ dBi, $P_t = 10$ dBm, $\sigma^2 = -174$ dBm/Hz, $B = 20$ GHz, $S = 20$, $f_c = 300$ GHz, $L_x = L_y = \lambda/2$, $\mathbf{p}_t = (x_t, y_t, z_t) = (0.8, -0.8, 0.2)$, and $\mathbf{p}_r = (x_r, y_r, z_r) = (0.8, r_r, 0.2)$.

We therefore formulate the optimization problem

$$\max_{\mathbf{b}} \sum_{s=0}^{S-1} |\mathbf{h}_s^T \mathbf{b}|^2 = \|\mathbf{H}^T \mathbf{b}\|^2 = \mathbf{b}^H \mathbf{H}^* \mathbf{H}^T \mathbf{b}, \quad (21)$$

where $\mathbf{H} = [\mathbf{h}_0, \dots, \mathbf{h}_{S-1}] \in \mathbb{C}^{N \times S}$. The above quadratic form has the solution $\mathbf{b}^* = \sqrt{N} \mathbf{u}$, where \mathbf{u} is the unit-norm eigenvector corresponding to the maximum eigenvalue of the Hermitian matrix $\mathbf{H}^* \mathbf{H}^T$. Since the elements of \mathbf{b}^* do not satisfy the unit-modulus constraint, this solution is referred to as *upper bound optimization*; recall that \mathbf{b}^* would be implemented by controlling the amplitude and phase of each reflection coefficient, which is not feasible in the passive IRS architecture under consideration. As a result, the upper bound optimization serves as a benchmark to assess the impact of the spatial-wideband effect on the achievable rate. In Fig. 2(b), the achievable rates of the frequency-dependent beamfocusing, narrowband beamfocusing, and upper bound optimization approach are 52.48 Gbps, 14.52 Gbps, and 24.61 Gbps, respectively. Narrowband beamfocusing performs very poor, and results in a 72.3% rate loss. Moreover, the upper bound optimization approach performs better, yet yields a much smaller rate than frequency-dependent beamfocusing. This numerical experiment showcases the importance of having IRS elements with a wideband response [21].

C. Energy Efficiency

1) *MIMO System*: Consider a MIMO system, where the Tx and Rx have N_t and N_r antennas, respectively. For efficient hardware implementation, hybrid analog-digital array architectures are assumed at both ends. The frequency-dependent path loss of the direct channel, i.e., line-of-sight (LoS), is [5]

$$\text{PL}_{\text{MIMO}}(f) = \frac{G_t G_r c^2}{(4\pi r_d (f_c + f))^2} e^{-\kappa_{\text{abs}}(f) r_d}, \quad (22)$$

where $r_d = \|\mathbf{p}_t - \mathbf{p}_r\|$. Next, we assume that N_t and N_r are adequately small so that the spatial-wideband effect is negligible; this can be attained by a uniform planar array (UPA), such as an 10×10 -element UPA [5]. In the far-field, the LoS channel matrix is rank-one; this holds for all distances larger than the Fraunhofer distance $2D_m^2/\lambda$, where D_m is the maximum dimension of the antenna array and λ is the carrier wavelength [22, Ch. 7]. Then, frequency-flat beamforming and combining yield the received SNR

$$\text{SNR}_s^{\text{MIMO}} = \frac{N_t N_r P_t \text{PL}_{\text{MIMO}}(f_s)}{B \sigma^2}. \quad (23)$$

The respective power consumption is calculated as²

$$P_{\text{MIMO}} = P_t + N_r (P_{\text{PS}} + P_{\text{PA}}) + N_t (P_{\text{PS}} + P_{\text{PA}}), \quad (24)$$

where P_{PS} and P_{PA} are the power consumption values for a phase shifter and a power amplifier, which are 42 mW and 60 mW at $f_c = 300$ GHz, respectively [3].

2) *IRS-Aided MIMO System*: The Tx and Rx perform beamforming and combining to communicate a single stream through the IRS of N elements. Due to the directional transmissions, the Tx-Rx link is very weak, and hence is neglected. In this case, the received SNR at the s th OFDM subcarrier is

$$\text{SNR}_s = \frac{N_t N_r N^2 G_s P_t \text{PL}(f_s)}{B \sigma^2}. \quad (25)$$

Using varactor diodes, the power expenditure of an IRS element is nearly negligible [13]. For the sake of exposition, we assume that the power consumption of the IRS-aided system is also given by (24). Therefore, the energy efficiency (EE) is given by $\sum_{s=0}^{S-1} \frac{B}{S} \log_2(1 + \text{SNR}_s) / P_{\text{MIMO}}$. Akin to [4], we can now decrease the number of antennas as N_t/α

²The power consumption of signal processing is neglected.

and N_r/α , whilst increasing the number of IRS elements as $N^* = \alpha \frac{\lambda}{L_x L_y} \frac{r_t r_r}{\sqrt{F(\theta_t, \phi_r, \theta_r) r_d}} e^{-\frac{1}{2} \kappa_{\text{abs}}(f)(r_d - r_r - r_t)}$, to attain an EE gain α compared to the pure MIMO system. The achievable rate, EE, and N^* are plotted versus r_r in Fig. 3. In contrast to the spatially narrowband case, IRS-assisted MIMO cannot outperform MIMO because of the beam squint effect present in the former architecture.

IV. CONCLUSIONS

We have studied, for the first time, the spatial-wideband effect in IRS-aided THz communications. In particular, we introduced a spherical wave channel model that captures the peculiarities of wideband transmissions. Capitalizing on the proposed channel model, we analyzed the power gain for both discrete and continuous IRSs under narrowband beam-focusing. Our results demonstrate that frequency-dependent beamfocusing is crucial to the successful deployment of future IRS-assisted wideband THz systems. Regarding future work, it would be interesting to model each IRS element as a transmission line and investigate the wideband design problem. Another promising direction would be to consider the mutual coupling between closely-spaced reflecting elements and its impact on system performance [23].

ACKNOWLEDGEMENTS

This project has received funding from the European Research Council (ERC) under the European Union's Horizon 2020 research and innovation programme (grant agreement No. 101001331).

APPENDIX

We have that

$$\frac{\sum_{n=-\frac{N_x}{2}}^{\frac{N_x}{2}-1} \sum_{m=-\frac{N_y}{2}}^{\frac{N_y}{2}-1} e^{-j2\pi f_s \frac{\tilde{r}_t(n,m) + \tilde{r}_r(n,m)}{c}} L_x L_y}{(N_x L_x)(N_y L_y)} \approx \frac{\int_{-\frac{\tilde{L}_x}{2}}^{\frac{\tilde{L}_x}{2}} \int_{-\frac{\tilde{L}_y}{2}}^{\frac{\tilde{L}_y}{2}} e^{-j2\pi f_s \frac{\tilde{r}_t(n,m) + \tilde{r}_r(n,m)}{c}} dx dy}{\tilde{L}_x \tilde{L}_y}, \quad (26)$$

where $\tilde{L}_x = N_x L_x$, $\tilde{L}_y = N_y L_y$, $dx = L_x$, and $dy = L_y$. Now setting $(n - 1/2)L_x = x$ and $(m - 1/2)L_y = y$ in $\tilde{r}_t(n, m)$ and $\tilde{r}_r(n, m)$, and leveraging the identity

$$\int e^{-jk(ax^2 - bx)} dx = \frac{\sqrt{\pi}}{2\sqrt{jka}} \text{erf} \left(\sqrt{jka} \left(x - \frac{b}{2a} \right) \right) \quad (27)$$

gives the desired result after basic algebra.

REFERENCES

- [1] T. S. Rappaport *et al.*, "Wireless communications and applications above 100 GHz: Opportunities and challenges for 6G and beyond," *IEEE Access*, vol. 7, pp. 78729-78757, 2019.
- [2] J. Zhang *et al.*, "Prospective multiple antenna technologies for beyond 5G," *IEEE J. Sel. Areas Commun.*, vol. 38, no. 8, pp. 1637-1660, Aug. 2020.
- [3] L. Yan, C. Han, and J. Yuan, "A dynamic array-of-subarrays architecture and hybrid precoding algorithms for terahertz wireless communications," *IEEE J. Sel. Areas Commun.*, vol. 38, no. 9, pp. 2041-2056, Sept. 2020.

- [4] K. Dovelos, S. D. Assimonis, H. Q. Ngo, B. Bellalta, and M. Matthaiou, "Intelligent reflecting surfaces at terahertz bands: Channel modeling and analysis," in *Proc. IEEE ICC*, Jun. 2021, pp. 1-6.
- [5] K. Dovelos, M. Matthaiou, H. Q. Ngo, and B. Bellalta, "Channel estimation and hybrid combining for wideband terahertz massive MIMO systems," *IEEE J. Sel. Areas Commun.*, vol. 39, no. 6, pp. 1604-1620, Jun. 2021.
- [6] S. Ma, W. Shen, J. An, and L. Hanzo, "Wideband channel estimation for IRS-aided systems in the face of beam squint," *IEEE Trans. Wireless Commun.*, Apr. 2021.
- [7] Y. Chen, D. Chen, and T. Jiang, "Beam-squint mitigating in reconfigurable intelligent surface aided wideband mmWave communications," in *Proc. WCNC*, May 2021, pp. 1-6.
- [8] B. Ning *et al.*, "Terahertz multi-user massive MIMO with intelligent reflecting surface: Beam training and hybrid beamforming," *IEEE Trans. Veh. Technol.*, vol. 70, no. 2, pp. 1376-1393, Feb. 2021.
- [9] E. Björnson and L. Sanguinetti, "Power scaling laws and near-field behaviors of massive MIMO and intelligent reflecting surfaces," *IEEE Open J. Commun. Soc.*, vol. 1, pp. 1306-1324, 2020.
- [10] A.-A. A. Boulogeorgos and A. Alexiou, "Coverage analysis of reconfigurable intelligent surface assisted THz wireless systems," *IEEE Open J. Veh. Technol.*, vol. 2, pp. 94-110, Jan. 2021.
- [11] Ö. Özdoğan, E. Björnson, and E. G. Larsson, "Intelligent reflecting surfaces: Physics, propagation, and pathloss modeling," *IEEE Wireless Commun. Lett.*, vol. 9, no. 5, pp. 581-585, May 2020.
- [12] M. Najafi, V. Jamali, R. Schober, and H. V. Poor, "Physics-based modeling and scalable optimization of large intelligent reflecting surfaces," *IEEE Trans. Commun.*, vol. 69, no. 4, pp. 2673-2691, Apr. 2021.
- [13] W. Tang *et al.*, "Wireless communications with reconfigurable intelligent surface: Path loss modeling and experimental measurement," *IEEE Trans. Wireless Commun.*, vol. 20, no. 1, pp. 421-439, Jan. 2021.
- [14] B. Zheng and R. Zhang, "Intelligent reflecting surface-enhanced OFDM: Channel estimation and reflection optimization," *IEEE Wireless Commun. Lett.*, vol. 9, no. 4, pp. 518-522, Apr. 2020.
- [15] Y. Yang, B. Zheng, S. Zhang, and R. Zhang, "Intelligent reflecting surface meets OFDM: Protocol design and rate maximization," *IEEE Trans. Commun.*, vol. 68, no. 7, pp. 4522-4535, Jul. 2020.
- [16] S. Lin *et al.*, "Adaptive transmission for reconfigurable intelligent surface-assisted OFDM wireless communications," *IEEE J. Sel. Areas Commun.*, vol. 38, no. 11, pp. 2653-2665, Nov. 2020.
- [17] Z. Wan, Z. Gao, M. Di Renzo, and M.-S. Alouini, "Terahertz massive MIMO with holographic reconfigurable intelligent surfaces," *IEEE Trans. Commun.*, Mar. 2021.
- [18] C. Huang *et al.*, "Holographic MIMO surfaces for 6G wireless networks: Opportunities, challenges, and trends," *IEEE Wireless Commun.*, vol. 27, no. 5, pp. 118-125, Oct. 2020.
- [19] C. Han and Y. Chen, "Propagation modeling for wireless communications in the terahertz band," *IEEE Commun. Mag.*, vol. 56, no. 6, pp. 96-101, Jun. 2018.
- [20] Y. Chen *et al.*, "Hybrid precoding for wideband millimeter wave MIMO systems in the face of beam squint," *IEEE Trans. Wireless Commun.*, vol. 20, no. 3, pp. 1847-1860, Mar. 2021.
- [21] S. M. A. Momeni Hasan Abadi *et al.*, "Ultra-wideband, true-time-delay reflectarray antennas using ground-plane-backed, miniaturized-element frequency selective surfaces," *IEEE Trans. Antennas Propag.*, vol. 63, no. 2, pp. 534-542, Feb. 2015.
- [22] D. Tse and P. Viswanath, *Fundamentals of Wireless Communication*. New York, NY, USA: Cambridge Univ. Press, 2005.
- [23] G. Gradoni and M. Di Renzo, "End-to-end mutual coupling aware communication model for reconfigurable intelligent surfaces: An electromagnetic-compliant approach based on mutual impedances," *IEEE Wireless Commun. Lett.*, vol. 10, no. 5, pp. 938-942, May 2021.